

Search for a light-charged Higgs in a two-Higgs-doublet type II seesaw model at the LHC

Chuan-Hung Chen^{1,*} and Takaaki Nomura^{2,†}

¹*Department of Physics, National Cheng-Kung University, Tainan 70101, Taiwan*

²*School of Physics, KIAS, Seoul 130-722, Korea*

(Dated: June 14, 2021)

Abstract

A charged Higgs in the type II two-Higgs-doublet model (THDM) has been bounded to be above a few hundred GeV by the radiative B decays. A Higgs triplet extension of the THDM not only provides an origin of neutrino masses and a completely new doubly-charged Higgs decay pattern, but it also achieves a light-charged Higgs with a mass of $\mathcal{O}(100)$ GeV through the new scalar couplings in the scalar potential. It was found that these light-charged Higgs decays depend on its mass m_{H^\pm} , $\tan \beta$, and mixing effect $\sin \theta_\pm$: at $\tan \beta = 1$, if $m_{H^\pm} > m_W + m_Z$, $\bar{b}bW^\pm$, $W^\pm Z$, and $\tau\nu$ are the main decay modes; however, if $m_{H^\pm} < m_W + m_Z$, the main decay modes are then $\bar{b}bW$ and $\tau\nu$, and at $\tan \beta = 30$, the $\tau\nu$ mode dominates the other decays. When $m_t > m_{H^\pm} + m_b$, we found that the ATLAS and CMS recent upper bounds on the product of $BR(t \rightarrow H^+ b)BR(H^+ \rightarrow \tau^+ \nu)$ can be directly applied and will give a strict constraint on the correlation of m_{H^\pm} and $\sin \theta_\pm$. If the upper bound of $BR(t \rightarrow H^+ b)BR(H^+ \rightarrow \tau^+ \nu)$ is satisfied (escaped) for $m_t > (<)m_{H^\pm} + m_b$, it was found that the significance of discovering the charged Higgs through $H^\pm \rightarrow W^\pm Z$ is much lower than that through $H^\pm \rightarrow \bar{b}bW^\pm$. With a luminosity of 100 fb^{-1} at $\sqrt{s} = 13 \text{ TeV}$ and including the experimental bounds, the significance of the $H^\pm \rightarrow \bar{b}bW^\pm$ signal can reach around $6.2(2.4)\sigma$ for $m_{H^\pm} < (>)m_W + m_Z$.

*Electronic address: physchen@mail.ncku.edu.tw

†Electronic address: nomura@kias.re.kr

The two-Higgs-doublet model (THDM) is one of the minimal extensions of the standard model (SM) in supersymmetric (SUSY) and non-SUSY frameworks. The scalar bosons in the model comprise two CP-even scalars (h, η^0), one CP-odd pseudoscalar (χ^0), and two charged Higgs particles (η^\pm). To avoid the flavor-changing neutral currents at the tree level, a discrete symmetry is usually imposed. Thus, several types of non-SUSY THDMs have been classified in the literature according to the couplings to the fermions in the Yukawa sector [1, 2]; As such, different types of THDMs may have different constraints on their masses and couplings.

With the discovery of a new scalar via ATLAS [3] and CMS [4], the mass of the SM-like Higgs h was determined to be $m_h \approx 125$ GeV. Without fine-tuning the parameters in the scalar potential, the 2×2 mass-square matrix (M^2) elements of the CP-even scalars are expected to have the same order of magnitude. Due to the sizable off-diagonal entries of M^2 , the mass-splitting between the two CP-even Higgs bosons can reach a few hundred GeV. For instance, if the diagonal and off-diagonal elements of M^2 are 500^2 GeV 2 and 300^2 GeV 2 , respectively, then the masses of the CP-even bosons would be 126 GeV and 583 GeV.

Among the classifications of the model, only the type II THDM has the same Yukawa couplings as the minimal supersymmetric standard model (MSSM). It is of importance that the charged Higgs mass of this model is bounded to be $m_{\eta^\pm} > 480$ GeV at the 95% confidence level (CL) [5] by the precision measurement of $B \rightarrow X_s \gamma$ [6]. Additionally, the constraint is insensitive to the parameter $\tan \beta = v_2/v_1$, where $v_{1(2)}$ is the vacuum expectation value (VEV) of the Higgs doublet that couples to the up(down)-type quarks. As a result, the charged Higgs in the type II THDM can not be a light particle unless the model is further extended.

One of the unsolved puzzles in particle physics is the origin of neutrino masses. If we assume that the neutrino mass arises from spontaneous symmetry breaking (SSB), like that in the SM and THDM, the minimal extension of the THDM adds an $SU(2)$ Higgs triplet Δ [7, 8]. In addition to the new scalar bosons, such as doubly-charged Higgses $\delta^{\pm\pm}$ and neutral scalars (δ^0, ξ^0), a pair of new charged scalar bosons δ^\pm exists in such models. Due to the strict constraint from the precision measurement of the electroweak ρ -parameter [6], the VEV of Δ (v_Δ) is limited to $v_\Delta < 3.4$ GeV. That is, before electroweak symmetry breaking (EWSB), the triplet-scalar bosons are degenerated massive particles. It can be easily seen that if only one Higgs doublet and one Higgs triplet are involved in a model,

e.g. the so-called type-II seesaw model [7, 8], the mass-splittings among the Higgs-triplet components are suppressed by v_Δ/m_Δ , where m_Δ is the typical mass of the Higgs triplet. By assuming that $\delta^{\pm\pm}$ are 100% decayed into leptons, the experimental lower bound on the m_Δ is currently around 400 GeV [12, 13].

Some interesting characteristics in the two-Higgs-doublet (THD) type II seesaw model have been reported [9, 10]: (i) the mass-splittings among the triplet components can be of the $\mathcal{O}(m_W)$; (ii) the doubly-charged Higgses $\delta^{\pm\pm}$ have a completely new dominant decay pattern, e.g., $\delta^{\pm\pm} \rightarrow H^\pm H^\pm$, where H^\pm are the lightest singly charged Higgses; and, (iii) the H^\pm can be as light as $\mathcal{O}(100)$ GeV. These characteristics are ascribed to the new interactions in the scalar potential, which are summarized as [9, 10]:

$$V(\Phi_1, \Phi_2, \Delta) \supset \mu_1 \Phi_1^T i\tau_2 \Delta^\dagger \Phi_1 + \mu_2 \Phi_2^T i\tau_2 \Delta^\dagger \Phi_2 + \mu_3 \Phi_1^T i\tau_2 \Delta^\dagger \Phi_2 + h.c. , \quad (1)$$

where $\Phi_{1,2}$ are the Higgs doublets; τ_2 is the second Pauli matrix, and $\mu_{1,2,3}$ are the mass dimension-one parameters and can be on the order of an electroweak scale. The VEV of Δ can then be simplified as:

$$v_\Delta \sim \frac{1}{\sqrt{2}m_\Delta^2} (\mu_1 v_1^2 + \mu_2 v_2^2 + \mu_3 v_1 v_2) , \quad (2)$$

the detailed expression of which can be found in [9]. As a result, the small v_Δ can be achieved by taking proper values of $\mu_{1,2,3}$. According to the results of $\mu_{1,2,3} \sim \mathcal{O}(m_W)$, the off-diagonal singly-charged Higgs mass-square matrix can be compatible with $m_{\eta^\pm}^2$ and m_Δ^2 ; and following the earlier discussion on the case of the two CP-even bosons, one indeed can obtain the light-charged Higgs with a mass of 100 GeV, even $m_\Delta \sim m_\eta^\pm \sim 500$ GeV. The only consequence is to introduce a mixing effect between η^\pm and δ^\pm . Since the doubly-charged Higgs of the Higgs triplet does not mix with other particles, its mass is $m_{\delta^{\pm\pm}} \approx m_\Delta$. A detailed analysis for $\delta^{\pm\pm}$ production at the LHC in this model can be found in [10].

Direct searches for a light-charged Higgs were performed at the LHC with $\sqrt{s} = 7$ TeV [14–17] and 8 TeV [18–20]. Although significant events above the background have not yet been found, the search for a light-charged Higgs still continues and remains an interesting issue at the LHC [21–23]. Based on the characteristics of the THD type II seesaw model, in this work, we study the possible signatures of the light-charged Higgs at the LHC. Since the triplet-charged Higgses δ^\pm can couple to $W^\mp Z$ at the tree level, the decays of $H^\pm \rightarrow W^\pm Z$ are sizable when $m_{H^\pm} > m_W + m_Z$; therefore, we separated the light-charged Higgs mass

into two ranges , namely (I) $m_W + m_Z \leq m_{H^\pm} < m_t + m_b$ and (II) $m_{H^\pm} < m_W + m_Z$, where the light-charged Higgs predominantly decays to $\bar{b}bW$, WZ , $\tau\nu$, and cs in the former range and decays to $\bar{b}bW$, $\tau\nu$, and cs in the latter range. It is worth mentioning that if the pseudoscalar A^0 of the THD is lighter than the charged Higgs, the $H^\pm \rightarrow W^\pm A^0$ decay may become the dominant decay channel. Since we do not have any information about the mass of the pseudoscalar boson (A^0), we omit the discussions of the $H^\pm \rightarrow W^\pm A^0$ decays by assuming $m_{A^0} > m_{H^\pm}$ in the study range of m_{H^\pm} . This assumption is supported by the recent CMS measurement, in which the mass m_{A^0} in the range $20 - 270$ GeV at small $\tan\beta$ was excluded [25]. Although the $H^\pm \rightarrow W^\pm h$ decays could be interesting processes to investigate the charged Higgs, the vertices are suppressed by $\cos(\beta - \alpha)$, which has been strictly limited by the current Higgs data [11]. While it is not necessary, for simplicity, we adopt $\cos(\beta - \alpha) \approx 0$ in this analysis.

In order to study the light-charged Higgs production and decays, we briefly introduce the relevant mixing and couplings in the following. As discussed earlier, the singly-charged Higgses, namely η^\pm and δ^\pm , can mix together due to the interactions in Eq. (1). We parameterize the physically-charged Higgs states as:

$$\begin{pmatrix} H_1'^\pm \\ H^\pm \end{pmatrix} = \begin{pmatrix} \cos\theta_\pm & \sin\theta_\pm \\ -\sin\theta_\pm & \cos\theta_\pm \end{pmatrix} \begin{pmatrix} \eta^\pm \\ \delta^\pm \end{pmatrix}, \quad (3)$$

where $H^\pm (H'^\pm)$ are identified as the lighter (heavier) charged Higgses. Accordingly, the Yukawa couplings of H^\pm to the SM quarks are given by:

$$\mathcal{L}_Y^{H^\pm} = -\sqrt{2} \sin\theta_\pm \bar{u} \left[\frac{t_\beta}{v} \mathbf{V} \mathbf{m}_d P_R + \frac{1}{v t_\beta} \mathbf{m}_u \mathbf{V} P_L \right] dH^+ + h.c., \quad (4)$$

in which we have suppressed the flavor indices, and where \mathbf{V} denotes the Cabibbo-Kobayashi-Maskawa (CKM) matrix, and $t_\beta = \tan\beta$. One can easily obtain the lepton Yukawa couplings if the quark masses and CKM matrix are respectively replaced by the lepton masses and Pontecorvo-Maki-Nakagawa-Sakata (PMNS) matrix. It is clear that the radiative B decaying via the charged Higgs can be suppressed by $\sin^2\theta_\pm$ in the decay amplitude; in this manner, the constraint on the light-charged Higgs is relaxed. We then write the Feynman rules for

the gauge interactions as:

$$\begin{aligned}
Z\chi^+\chi^- &: \frac{gc_\chi}{2c_W}(p_+^\mu - p_-^\mu), \\
A\chi^+\chi^- &: e(p_+^\mu - p_-^\mu), \\
WZ\delta^\pm &: -\frac{g^2 v_\Delta}{\sqrt{2}c_W} g^{\mu\nu}, \tag{5}
\end{aligned}$$

where we have used the basis of η^\pm and δ^\pm instead of H^\pm and H'^\pm , χ^\pm represent η^\pm and δ^\pm , and p_\pm^μ denote the momenta of the charged particles, $c_W(s_W) = \cos \theta_W (\sin \theta_W)$, $c_\eta = 1 - 2s_W^2$, and $c_\delta = -s_W^2$. It can be seen that the W^-ZH^+ coupling is suppressed by v_Δ/v ; however, when $t_\beta \sim \mathcal{O}(1)$, its magnitude is compatible with the $m_\tau t_\beta/v$ coupling of $\tau\nu H^+$. Thus, in the (I) mass range, the relative branching ratios (BRs) for $H^\pm \rightarrow W^\pm Z$ and $H^\pm \rightarrow \tau\nu$ are sensitive to the $\sin \theta_\pm$.

After introducing the relevant couplings, we then study the partial decay rates of the charged Higgs for the kinematically-allowed channels. It was found that in the (I) mass range, the partial-decay rate indeed is dominated by the three-body decay $H^+ \rightarrow \bar{b}t^* \rightarrow \bar{b}bW^+$, the expression of which is written as:

$$\begin{aligned}
\Gamma(H^\pm \rightarrow \bar{b}bW^\pm) &\approx \frac{N_c g^2 s_\pm^2}{2m_{H^\pm}} \int_{(m_W+m_b)^2}^{(m_{H^\pm}-m_b)^2} \left| \frac{1}{q^2 - m_t^2 - i\Gamma_t m_t} \right|^2 \\
&\times \left[\left(\frac{m_b^2 t_\beta^2}{v^2} + \frac{m_t^2}{q^2} \frac{m_t^2}{v^2 t_\beta^2} \right) p_H \cdot p_{b1} + 2 \frac{m_b^2 m_t^2}{v^2} \right] \\
&\times \left[2p_t \cdot p_{b2} + \frac{1}{m_W^2} \left((q^2 - m_b^2)^2 - m_W^4 \right) \right] d_3(PS), \tag{6}
\end{aligned}$$

where $p_H \cdot p_{b1}$ and $p_t \cdot p_{b2}$ are the inner products of the particle momenta, and $d_3(PS)$ denotes the phase space factor of the three-body decay. In sum, they are given by:

$$\begin{aligned}
p_H \cdot p_{b1} &= \frac{1}{2} (m_H^2 - q^2 - m_b^2), \quad p_t \cdot p_{b2} = \frac{1}{2} (q^2 - m_W^2 + m_b^2), \\
d_3(PS) &= \frac{dq^2}{(2\pi)^5} \left(\frac{\pi}{m_{H^\pm}} \sqrt{E_{b1}^2 - m_b^2} \right) \left(\frac{\pi}{\sqrt{q^2}} \sqrt{E_W^2 - m_W^2} \right), \\
E_{b1} &= \frac{m_{H^\pm}^2 - q^2 + m_b^2}{2m_{H^\pm}}, \quad E_W = \frac{q^2 + m_W^2 - m_b^2}{2\sqrt{q^2}}. \tag{7}
\end{aligned}$$

Meanwhile, the dominant two-body decays are formulated as:

$$\begin{aligned}\Gamma(H^\pm \rightarrow \tau\nu) &\approx \frac{m_{H^\pm}}{8\pi} \left(s_\pm \frac{m_\tau t_\beta}{v} \right)^2 \left(1 - \frac{m_\tau^2}{m_{H^\pm}^2} \right)^2, \\ \Gamma(H^\pm \rightarrow cs) &\approx \frac{N_c s_\pm^2 m_{H^\pm}}{8\pi} \left(\frac{m_s^2 t_\beta^2}{v^2} + \frac{m_c^2}{v^2 t_\beta^2} \right) \left(1 - \frac{m_c^2}{m_{H^\pm}^2} \right)^2, \\ \Gamma(H^\pm \rightarrow W^\pm Z) &\approx \frac{g^4 c_\pm^2 v_\Delta^2}{32\pi c_W^2 m_{H^\pm}} \sqrt{\lambda(r_Z, r_W)} \left[2 + \frac{(m_{H^\pm}^2 - m_Z^2 - m_W^2)^2}{4m_Z^2 m_W^2} \right],\end{aligned}\quad (8)$$

in which the light fermion masses were dropped, and $V_{cs} \approx 1$ is used; and where $s_\pm(c_\pm) = \sin \theta_\pm(\cos \theta_\pm)$; $r_Z = m_Z^2/m_{H^\pm}^2$, $r_W = m_W^2/m_{H^\pm}^2$, and $\lambda(a, b) = (1 + a - b)^2 - 4a$. In addition to the $\tau\nu$ and cs modes, in the (II) mass range one of the vector bosons in the vector-boson pair channels becomes off-shell. Although the contributions of the off-shell channels are small, their partial decay rates are still expressed as follows:

$$\begin{aligned}\Gamma(H^\pm \rightarrow ZW^{\pm*}) &\approx \frac{3g^6 v_\Delta^2 c_\pm^2}{2^8 \pi^3 c_W^2} \int_0^{\Delta M_Z^2} dq^2 \frac{q^2 \sqrt{\lambda(r_Z, r_q)}}{|q^2 - m_W^2|^2} \left[1 + \frac{E^2(m_Z^2, q^2)}{2m_Z^2} \right], \\ \Gamma(H^\pm \rightarrow W^\pm Z^*) &\approx \frac{g^6 v_\Delta^2 c_\pm^2 \xi_{VA}}{9 \cdot 2^8 \pi^3 c_W^4} \int_0^{\Delta M_W^2} dq^2 \frac{q^2 \sqrt{\lambda(r_W, r_q)}}{|q^2 - m_Z^2|^2} \left[1 + \frac{E^2(m_W^2, q^2)}{2m_W^2} \right]\end{aligned}\quad (9)$$

where $\Delta M_V^2 = (m_{H^\pm} - m_V)^2$, $\xi_{VA} = 63/2 + 20s_W^2(4s_W^2 - 3)$, and $E(m^2, q^2) = (m_{H^\pm}^2 - m^2 - q^2)/(2\sqrt{q^2})$.

According to the obtained formulas for the H^\pm decays, we show the BR for each H^\pm decay mode as a function of m_{H^\pm} in Fig. 1(a) and as a function of s_\pm in Fig. 1(b), where $s_\pm = 0.4$ and $m_{H^\pm} = 175$ GeV are used in plots (a) and (b), respectively, $t_\beta = 1$ is fixed in both plots, and $F_{1,2}$ in the y-axis denote the possible final states. Other taken values of parameters are shown in Table I. Without further elaboration, $v_\Delta = 3$ GeV is indicated in this work. Since the W/Z gauge boson can be off-shell and on-shell in the H^\pm decays when m_{H^\pm} is taken as a variable, to include the effects of the W/Z -gauge boson width, the $BR(H^\pm \rightarrow W^{\pm(*)}Z^{(*)})$ is calculated by summing over all possible W/Z decays, i.e. $BR(H^\pm \rightarrow W^{\pm(*)}Z^{(*)}) = \sum_{f_1, f_2, f_3, f_4} BR(H^\pm \rightarrow f_1 f_2 f_3 f_4)$, where f_i s denotes all possible final states. Here, we employ CalcHEP [26] with a narrow-width approximation to estimate the numerical values for the $BR(H^\pm \rightarrow W^{\pm(*)}Z^{(*)})$. For simplicity, we hereafter use WZ instead of $W^{\pm(*)}Z^{(*)}$.

From plot (a), it can be clearly seen that when $m_{H^\pm} > 160$ GeV, the $BR(H^\pm \rightarrow \bar{b}bW^\pm)$ is one order of magnitude larger than the other decay modes. The $BR(H^\pm \rightarrow \tau\nu)$ is about two-fold larger than the $BR(H^\pm \rightarrow cs)$ in both the (I) and (II) mass ranges. When

| $m_t(pole)$ | $m_b(m_b)$ | m_W | m_Z | Γ_t | Γ_W | Γ_Z |
|-------------|------------|-------|-------|------------|------------|------------|
| 173 | 4.2 | 80.39 | 91.19 | 1.41 | 2.11 | 2.52 |

TABLE I: Inputs of particle masses and widths in units of GeV.

$m_{H^\pm} > m_W + m_Z$, the BRs of the $\tau\nu$ and WZ decay channels are compatible. From plot (b), it can be seen that the $BR(H^\pm \rightarrow WZ)$ is enhanced when s_\pm is decreased. On the other hand, since s_\pm dictates the single-charged Higgs production cross-section, in order to produce H^\pm bosons with sizable cross-sections, the values of s_\pm must not be too small. In order to clarify the situation with large values of t_β , we present the results with $t_\beta = 30$ in Fig. 2. From the results, it can clearly be seen that the $\tau\nu$ mode overwhelmingly dominates with large t_β .

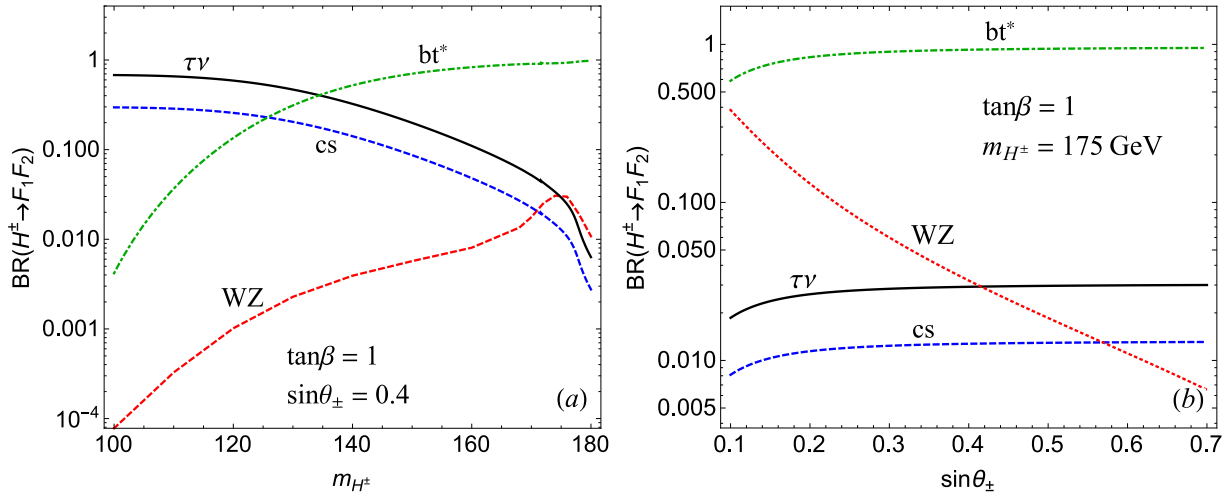


FIG. 1: BRs for the light-charged Higgs decays as a function of (a) m_{H^\pm} and (b) $\sin \theta_\pm$, where $\tan \beta = 1$ for both plots, bt^* stands for $\bar{b}bW$, $F_{1,2}$ denote the possible final states, and $\sin \theta_\pm = 0.4$ for plot (a), while $m_{H^\pm} = 175$ GeV for plot (b).

To numerically calculate the single-charged Higgs production cross-section, we use CalcHEP [26] associated with the CTEQ6L parton distribution functions (PDFs) [27]. The numerical analysis is conducted at the center of the mass energy of $\sqrt{s} = 13$ TeV. It was found that there are four channels of interest that could produce the single-charged Higgs in the pp collisions. They are: $H^+b\bar{t}$, $H^+\bar{t}$, H^+W^- , and H^++ jet, where the CP-conjugated processes are indicated, and the jet includes the gluon, light quarks, and b jets; further, their respective producing processes respectively are: $gg \rightarrow t\bar{t} \rightarrow H^+b\bar{t}$, $g\bar{b} \rightarrow H^+\bar{t}$, $q\bar{q} \rightarrow Z \rightarrow H^+W^-$, and

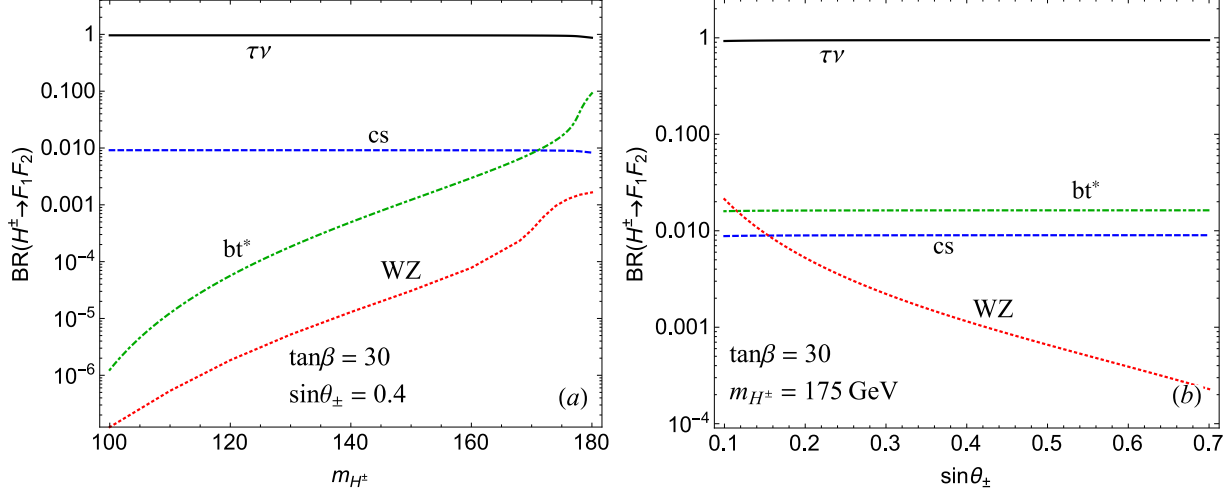


FIG. 2: This legend is the same as that in Fig. 1, except here $\tan \beta = 30$.

$gq \rightarrow H^+q'$ ($q, q' = u, d, s, c$). The main free parameters in this study are t_β , s_\pm , and m_{H^\pm} . To show the correlations between the cross-sections and m_{H^\pm} , the production cross-sections of these channels are plotted as a function of m_{H^\pm} in Fig. 3(a), in which $t_\beta = 1$ and $s_\pm = 0.4$. According to the results, we see that the cross-sections of the $H^+b\bar{t}$ and $H^+\bar{t}$ channels are much larger than those of the H^+W^- and H^+ jet channels. Similarly, the production cross-sections are shown as a function of s_\pm in Fig. 3(b), for which $t_\beta = 1$ and $m_{H^\pm} = 150$ GeV. It can be seen that when the values of s_\pm are around 0.2, both $\sigma(pp \rightarrow H^+b\bar{t})$ and $\sigma(pp \rightarrow H^+\bar{t})$ can still exceed 100 fb. From the results shown in Fig. 1(b), where the $BR(H^\pm \rightarrow WZ)$ is larger than the $BR(H^\pm \rightarrow \tau\nu)$ in the (I) mass region and small s_\pm , it is of interest to explore the charged Higgs through the WZ channel in such regions.

According to the charged Higgs-Yukawa couplings shown in Eq. (4), when t_β increases, the contributions from up(down)-type quarks decrease (increase). Since the $t(c)$ -quark is much heavier than the $b(s)$ -quark, it is expected that the single H^\pm production cross-sections would lower as the values of t_β initially augment. However, when the values of t_β increase up to m_t/m_b , due to $m_b t_\beta$ being near m_t and $m_s t_\beta$ being larger than m_c , the cross-sections are enhanced close to the case of $t_\beta = 1$. To illustrate the situation with a large t_β , we show the H^+ production cross-sections as a function of m_{H^\pm} and s_\pm , with $t_\beta = 30$ in Figs. 4(a) and (b), respectively. The plots show that only the H^+ jet channel has a significant enhancement, while the others are slightly smaller than when $t_\beta = 1$. The significant enhancement in the H^+ jet channel is due to the result of $m_s t_\beta > 2m_c$.

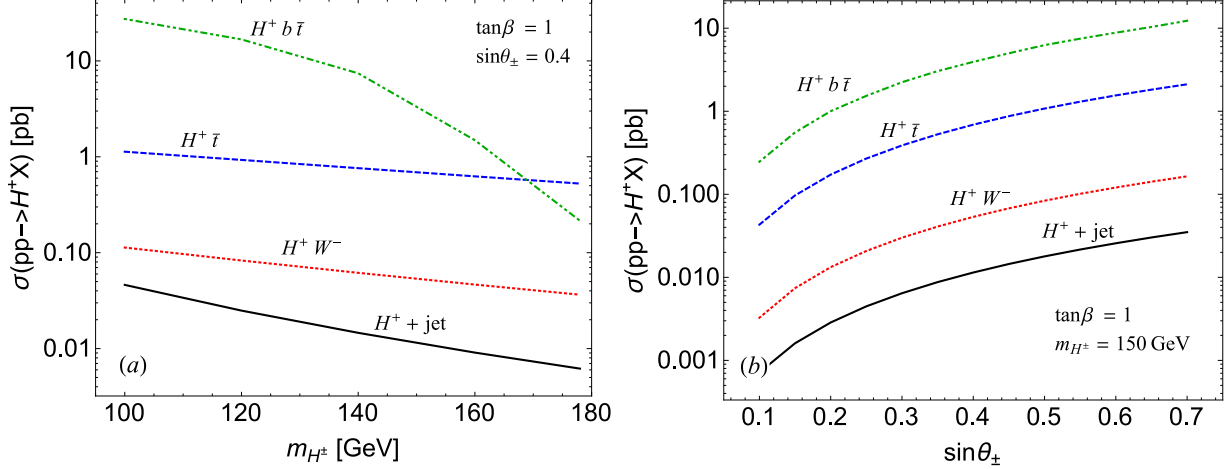


FIG. 3: Single-charged Higgs production cross-section at parton level via various channels as a function of (a) m_{H^\pm} and (b) $\sin \theta_\pm$, where $\sqrt{s} = 13$ TeV is used, we fixed $\tan \beta = 1$ for both plots, and $\sin \theta_\pm = 0.4$ for plot (a), while $m_{H^\pm} = 150$ GeV for plot (b).

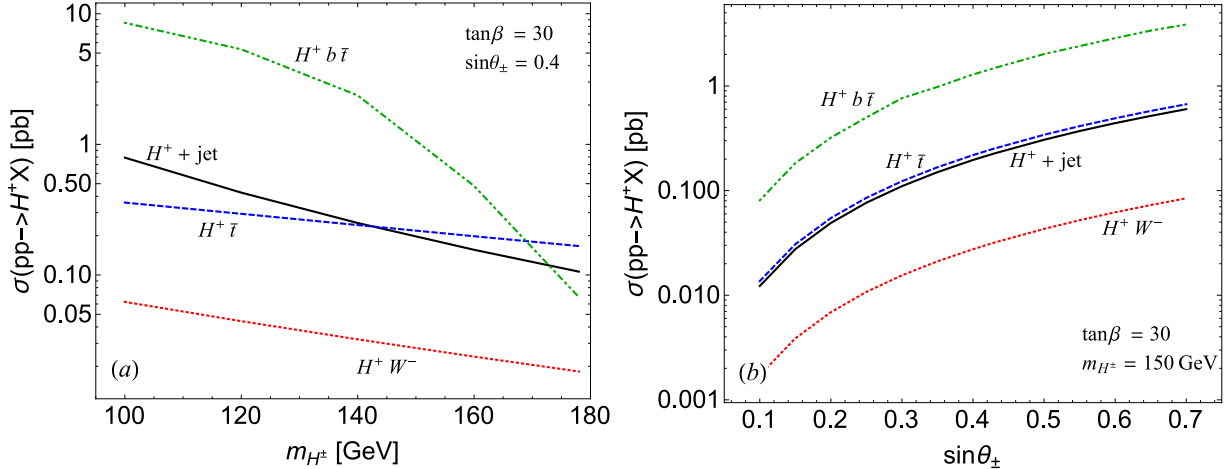


FIG. 4: This legend is the same as that in Fig. 3, except here $\tan \beta = 30$.

In order to assess the discovery potential of the light-charged Higgs, we employ the event generator `MadGraph5_aMC@NLO/MadEvent5` [29] to generate the simulation events, where the relevant Feynman rules and parameters of the model are provided by `FeynRules 2.0` [30], and the `NNPDF23L01` PDFs [32] are used. The generated events are passed through `PYTHIA 6` [31] to include the effects of hadronization and initial/final state radiation, and deal with the SM particle decays, e.g., the W -boson and top-quark decays. Furthermore, the events are also run through the `PGS 4` for detector simulation [33].

As aforementioned, the singly-charged Higgs H^\pm is predominantly produced by the pro-

cesses $pp \rightarrow H^\pm tb$, $pp \rightarrow H^\pm t$, and $pp \rightarrow H^\pm + \text{jet}$, while the production cross-sections and decays depend on the parameters m_{H^\pm} , s_\pm , and t_β . Therefore, to combine the charged Higgs (I, II) mass ranges with the $t_\beta = (1, 30)$ schemes, we classify the schemes as $S_{1A,1B}$ and $S_{2A,2B}$, where the number in the subscript denotes the mass range, and $A(B)$ represents $t_\beta = 1(30)$. We note that it encounters a double counting if we simply add up the events from the $pp \rightarrow H^\pm t$ and $pp \rightarrow H^\pm tb$ processes, where the events from the latter process may include those from the former process when the b -jet in the final state is collinear with the proton beam [34]. In order to remove the double counting effects, we apply MLM matching scheme [35, 36] which is implemented in `MadGraph5_aMC@NLO`. It is found that with $m_{H^\pm} = 175$ GeV, the matched cross-section for the $pp \rightarrow H^\pm t$ and $pp \rightarrow H^\pm tb$ channels is around 90% of that obtained by a simple sum of both channels. In addition, we also find that the double counting effects become weaker when the mass of charged Higgs is smaller. This behavior is consistent with that shown in [34]. Although we concentrate on the case of $m_{H^\pm} < m_t + m_b$, in order to avoid the double counting issue, we use the events which are generated by MadGraph with MLM matching procedure in the following analysis.

From Fig. 2, it can be seen that the decay $H^\pm \rightarrow \tau\nu$ dominates the other decay modes at large values of t_β ; that is, under such circumstances, $\tau\nu$ is the only channel that can be used to look for H^\pm . Recently, ATLAS [18] and CMS [20] reported the upper limits on the product of $BR(t \rightarrow H^+ b)BR(H^+ \rightarrow \tau^+\nu)$ at $\sqrt{s} = 8$ TeV. Accordingly, the experimental situation can be applied to our $S_{1B,2B}$ schemes. Thus, instead of performing an event simulation, we directly apply the constraints of the ATLAS and CMS measurements to the $S_{1B,2B}$ schemes when $m_t > m_{H^\pm} + m_b$ is satisfied. We note that although a stricter limit on m_{H^\pm} at $\sqrt{s} = 13$ TeV through $H^\pm \rightarrow \tau\nu$ was obtained by ATLAS [37], the mass range was for $m_{H^\pm} \geq 200$ GeV. Hence, we use the earlier results [18, 20] to constrain the parameters. According to the Yukawa couplings in Eq. (4), the decay width for $t \rightarrow H^+ b$ can be easily formulated as:

$$\Gamma_{t \rightarrow H^+ b} = \frac{m_t \sin^2 \theta_\pm}{16\pi} \sqrt{\lambda(x_{H^\pm}, x_b)} \left[(C_L^2 + C_R^2) \sqrt{\tilde{\lambda}(x_{H^\pm}, x_b)} + 4C_L C_R \frac{m_b}{m_t} \right], \quad (10)$$

$$C_L = \frac{m_t}{vt_\beta}, \quad C_R = \frac{t_\beta m_b}{v}, \quad \tilde{\lambda}(x, y) = 1 + x^2 + y^2 - 2x + 2y - 2xy,$$

in which $V_{tb} \approx 1$ is used, and where $x_{H^\pm} = m_{H^\pm}^2/m_t^2$, and $x_b = m_b^2/m_t^2$. To estimate the BR, the total top-quark decay width was taken as $\Gamma_t = 1.41$ GeV [28]. Consequently, we show the $BR(t \rightarrow H^+ b)BR(H^+ \rightarrow \tau^+\nu)$ as a function of m_{H^\pm} in Fig. 5, where the ATLAS (squares) and CMS (triangles) upper limits are shown in the plots. It should be noted that

the curves represent the different values of s_{\pm} , and for comparison, we plot the cases with $t_{\beta} = 1$ (left panel) and $t_{\beta} = 30$ (right panel). From the results, it can be seen that much of the parameter space of s_{\pm} was excluded by the current LHC data, with the constraint on the case with $t_{\beta} = 30$ being stronger due to the fact that $BR(H^+ \rightarrow \tau^+\nu) \approx 1$. In the following event simulation, we thus concentrate on the $S_{1A,2A}$ schemes.

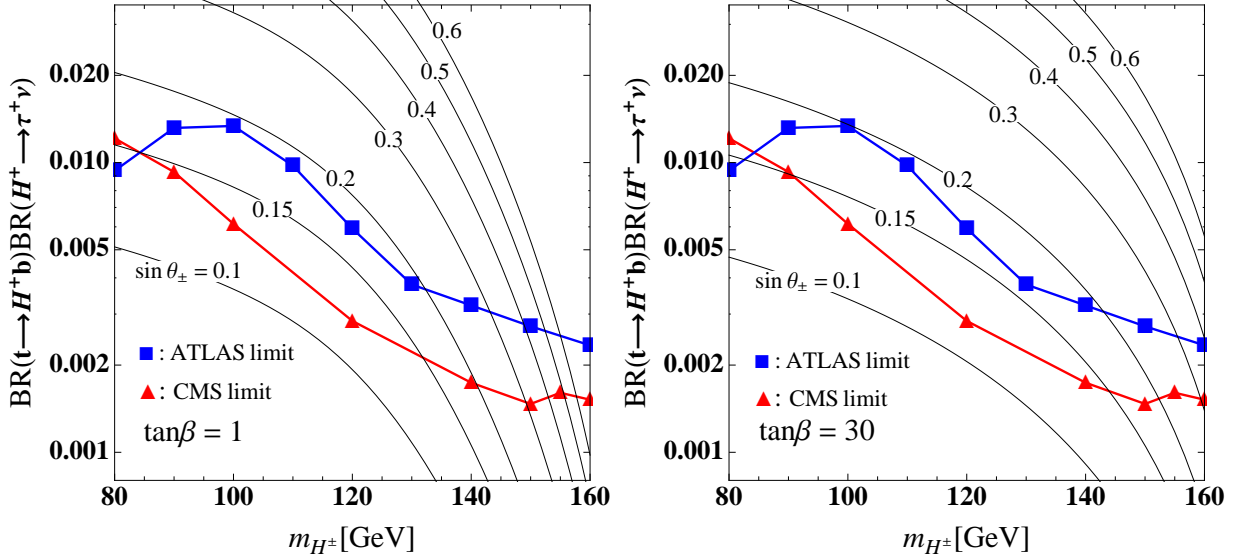


FIG. 5: Product of branching ratios $BR(t \rightarrow H^+b)BR(H^+ \rightarrow \tau^+\nu)$ as a function of $m_{H^{\pm}}$, where the upper limits from the ATLAS [18] and CMS [20] measurements are included; the curves represent the different values of s_{\pm} , and the left (right) panel is for $\tan\beta = 1(30)$.

To estimate the ratio of the signal event number (N_S) to the background event number N_B , we have to determine the SM backgrounds that can mimic the signals of the charged Higgs. The main background processes are listed as follows:

1. ZZ background: $pp \rightarrow ZZ + n \text{ jets}$,
2. WW background: $pp \rightarrow W^{\pm}W^{\mp} + n \text{ jets}$,
3. WZ background: $pp \rightarrow W^{\pm}Z + n \text{ jets}$,
4. top background: $pp \rightarrow t\bar{t}, t\bar{t}q(\bar{q}), t\bar{t}W^{\pm}$,

where the number of jets is assumed to be $n \leq 2$. In order to suppress the background events,

we consider the kinematic cuts (KCs), which are applied to all signals and backgrounds, as:

$$\begin{aligned} p_T(\ell) &> 20 \text{ GeV}, \quad \eta(\ell) < 2.5, \quad p_T(j_{\text{leading}}) > 50 \text{ GeV}, \\ p_T(j) &> 20 \text{ GeV}, \quad \eta(j) < 5.0, \end{aligned} \quad (11)$$

where p_T is the transverse momentum, $\eta = 1/2 \ln(\tan \theta/2)$ is the pseudo-rapidity with θ being the scattering angle in the laboratory frame, and j_{leading} denotes the highest p_T jet. Further cuts can be proposed depending on the properties of each process. In the following, we discuss the simulation analysis for each scheme.

Scheme S_{1A} : according to the results as shown in Fig. 1(b), it can be known that $H^+ \rightarrow W^+ Z/\bar{b}bW^+$ are the two main decay channels at small values of s_{\pm} . If we take $m_{H^{\pm}} = 175$ GeV, the signal processes of interest are

$$pp \rightarrow H^+ \bar{t}(H^+ \bar{t}b), \quad H^+ \rightarrow W^+ Z \text{ or } \bar{b}bW^+, \quad (12)$$

where CP-conjugated processes are also implied. To display the signal events for the $H^{\pm} \rightarrow b\bar{b}W^{\pm}$ and $H^{\pm} \rightarrow WZ$ channels, we set the extra event-selection conditions to be "2 leptons + n jets" and "3 leptons + m jets" with $n(m) \geq 4(3)$, respectively. And, to increase the significance of the signal from the $H^{\pm} \rightarrow WZ$ channel, we further require the invariant mass of the 3-lepton to satisfy the selection condition:

$$120 \text{ GeV} \leq M_{\ell^{\pm}\ell^+\ell^-} \leq 200 \text{ GeV}. \quad (13)$$

To clearly show the signal and each background, we present the event numbers after imposing the proposed KCs and extra selection conditions in Table II(III) for the $H^{\pm} \rightarrow WZ$ ($H^{\pm} \rightarrow \bar{b}bW^{\pm}$) signal and background, where the employed luminosity is 100 fb^{-1} . Note that the last column is the significance, which is defined as $S = N_S/\sqrt{N_B}$. Since the BR of the WZ mode can be higher than that of the $\tau\nu$ mode at small s_{\pm} , we take $s_{\pm} = 0.2$ for the $H^{\pm} \rightarrow WZ$ channel. However, in order to obtain a larger H^{\pm} production cross section, we take $s_{\pm} = 0.4$ for the $H^{\pm} \rightarrow \bar{b}bW^{\pm}$ channel. From Table II, it can be seen that with the proposed cuts, the background events from the top-quark and WZ backgrounds are still much larger than the signal events. In principle, we can further reduce the top-quark background by imposing the KC on the second highest p_T of the charged lepton; however, doing so does not significantly change the WZ background. The reason for this is that the kinematic distributions from the $H^{\pm} \rightarrow WZ$ signal and from the WZ background are very

similar. As such, the proposed KC will reduce both events. A similar situation also occurs, as shown in Table III, for the signal from the $H^\pm \rightarrow \bar{b}bW^\pm$ channel. The difference is that we can find a KC (e.g., invariant mass of $\ell^+\ell^-$) to reduce the WZ and ZZ backgrounds; nevertheless, due to the similarity in the kinematic distributions between the $H^\pm \rightarrow \bar{b}bW^\pm$ signal and top-quark background, finding an efficient cut that diminishes the top-quark background without reducing the signal is challenging.

From the results shown in both tables, it can be clearly seen that the significance from $H^\pm \rightarrow WZ$ is much smaller than that from $H^\pm \rightarrow \bar{b}bW^\pm$. The results can be easily understood as follows: the product of $\sigma(pp \rightarrow H^+t, H^+\bar{b}t)BR(H^+ \rightarrow W^+Z)$ at $s_\pm = 0.2$ is close to that at $s_\pm = 0.4$; however, $\sigma(pp \rightarrow H^+t, H^+\bar{b}t)BR(H^+ \rightarrow \bar{b}bW^+)$ at $s_\pm = 0.4$ is 30-fold larger than with $H^+ \rightarrow W^+Z$. By the definition of significance, the S of $H^\pm \rightarrow WZ$ natively should be one order of magnitude smaller than that of $H^\pm \rightarrow \bar{b}bW^\pm$. In sum, by combining all analyses, we conclude that it is difficult to search for a light -charged Higgs via the $H^\pm \rightarrow WZ$ channel.

| cuts | signal(3 ℓ) | $WW+nj$ | $ZZ+nj$ | $WZ+nj$ | top | top+ W | S |
|--------------------------------|-------------------|---------|-------------------|-------------------|-------------------|-------------------|------|
| KCs | 26. | 27. | 8.9×10^2 | 8.8×10^3 | 5.8×10^3 | 1.1×10^2 | 0.21 |
| $M_{\ell^\pm\ell^+\ell^-}$ cut | 19. | 9.0 | 40. | 5.1×10^3 | 3.2×10^3 | 50. | 0.15 |

TABLE II: Event number for the $H^\pm \rightarrow WZ$ signal and background with the proposed kinematic cuts in the scheme S_{1A} , where we have used the luminosity of 100 fb^{-1} , $m_{H^\pm} = 175 \text{ GeV}$, and $s_\pm = 0.2$.

| cuts | signal(2 ℓ) | $WW+nj$ | $ZZ+nj$ | $WZ+nj$ | top | top+ W | S |
|------|-------------------|-------------------|-------------------|-------------------|-------------------|-------------------|-----|
| KCs | 2.3×10^3 | 2.4×10^4 | 1.9×10^4 | 5.5×10^4 | 8.1×10^5 | 1.6×10^3 | 2.4 |

TABLE III: This legend is the same as that in Table II, except here for the $H^\pm \rightarrow \bar{b}bW^\pm$ signal and $s_\pm = 0.4$.

Scheme S_{2A} : in this scheme, it can be found from the plot shown in Fig. 1(a) that the charged Higgs mainly decays to $\tau\nu$ and $\bar{b}bW^\pm$, where the decay priority depends on m_{H^\pm} . For the case where $\tau\nu$ dominates, we can use the ATLAS and CMS measurements directly to constrain the parameters, as discussed earlier, for which the results are shown in Fig. 5. We

thus focus the simulation on the $\bar{b}bW^\pm$ channel by selecting some benchmark points (BPs) for the parameters instead of scanning all parameter spaces. Since the analysis is similar to that for scheme S_{1A} , we directly present the signal event numbers and significances with the selected BPs of (m_{H^\pm}, s_\pm) in Table. IV, and assumed the same luminosity, KCs, and backgrounds as those in Table III. In addition, the selected BPs satisfy the ATLAS [18] and CMS [20] upper limits shown in Fig. 5. From the table, it can be seen that a heavier H^\pm and larger s_\pm exhibit a greater significance. This is because when the H^\pm boson becomes heavier, in addition to the $BR(H^\pm \rightarrow \bar{b}bW^\pm)$ approaching unity, the larger allowed s_\pm values lead to larger single H^\pm production cross-sections.

| $(m_{H^\pm}[\text{GeV}], \sin \theta_\pm)$ | $(150, 0.2)$ | $(120, 0.1)$ | $(100, 0.1)$ |
|--|-------------------|-------------------|-------------------|
| # of events | 5.9×10^3 | 1.2×10^3 | 6.4×10^2 |
| S | 6.2 | 1.3 | 0.67 |

TABLE IV: Number of signal events and the associated significance with some selected benchmark points for the $H^\pm \rightarrow \bar{b}bW^\pm$ signal, where the luminosity, kinematic cuts and backgrounds are the same as those in Table III. The selected benchmark points satisfy the ATLAS [18] and CMS [20] upper limits on $BR(t \rightarrow H^+b)BR(H^+ \rightarrow \tau^+\nu)$.

In summary, we assessed the discovery potential of the light-charged Higgs in the two-Higgs-doublet and one-Higgs-triplet model at the center of a mass energy of $\sqrt{s} = 13$ TeV. If $H^\pm \rightarrow \tau\nu$ is the dominant decay channel, then the current ATLAS [18] and CMS [20] upper limits on the product of $BR(t \rightarrow H^+b)BR(H^+ \rightarrow \tau^+\nu)$ can be directly used, and the correlation between m_{H^\pm} and $\sin \theta_\pm$ is severely constrained. Although the $H^\pm \rightarrow WZ$ channel is allowed, and its branching ratio is not suppressed in the model, the significance of the $H^\pm \rightarrow WZ$ signal is much smaller than that of $H^\pm \rightarrow \bar{b}bW^\pm$. Accordingly, we conclude that the optimal better production processes to search for a light-charged Higgs are $pp \rightarrow H^+\bar{t}, H^+b\bar{t}$, for which the charged Higgs decay channel is $H^\pm \rightarrow \bar{b}bW^\pm$.

Acknowledgments

This work was partially supported by the Ministry of Science and Technology of Taiwan R.O.C., under grant MOST-103-2112-M-006-004-MY3 (CHC).

[1] G. C. Branco, P. M. Ferreira, L. Lavoura, M. N. Rebelo, M. Sher and J. P. Silva, Phys. Rept. **516**, 1 (2012) [arXiv:1106.0034 [hep-ph]].

[2] Y. H. Ahn and C. H. Chen, Phys. Lett. B **690**, 57 (2010) [arXiv:1002.4216 [hep-ph]].

[3] G. Aad *et al.* [ATLAS Collaboration], Phys. Lett. B **716**, 1 (2012) [arXiv:1207.7214 [hep-ex]].

[4] S. Chatrchyan *et al.* [CMS Collaboration], Phys. Lett. B **716**, 30 (2012) [arXiv:1207.7235 [hep-ex]].

[5] M. Misiak *et al.*, Phys. Rev. Lett. **114**, no. 22, 221801 (2015) [arXiv:1503.01789 [hep-ph]].

[6] K.A. Olive *et al.* (Particle Data Group), Chin. Phys. C, 38, 090001 (2014).

[7] M. Magg and C. Wetterich, Phys. Lett. B **94**, 61 (1980); G. Lazarides, Q. Shafi and C. Wetterich, Nucl. Phys. B **181**, 287 (1981); R. N. Mohapatra and G. Senjanovic, Phys. Rev. D **23**, 165 (1981); E. Ma and U. Sarkar, Phys. Rev. Lett. **80**, 5716 (1998) [hep-ph/9802445].

[8] W. Konetschny and W. Kummer, Phys. Lett. B **70**, 433 (1977); J. Schechter and J. W. F. Valle, Phys. Rev. D **22**, 2227 (1980); T. P. Cheng and L. -F. Li, Phys. Rev. D **22**, 2860 (1980); S. M. Bilenky, J. Hosek and S. T. Petcov, Phys. Lett. B **94**, 495 (1980).

[9] C. H. Chen and T. Nomura, Phys. Rev. D **90**, no. 7, 075008 (2014) [arXiv:1406.6814 [hep-ph]].

[10] C. H. Chen and T. Nomura, Phys. Rev. D **91**, 035023 (2015) [arXiv:1411.6412 [hep-ph]].

[11] R. Benbrik, C. H. Chen and T. Nomura, Phys. Rev. D **93**, no. 9, 095004 (2016) [arXiv:1511.08544 [hep-ph]].

[12] S. Chatrchyan *et al.* [CMS Collaboration], Eur. Phys. J. C **72**, 2189 (2012) [arXiv:1207.2666 [hep-ex]].

[13] G. Aad *et al.* [ATLAS Collaboration], Eur. Phys. J. C **72**, 2244 (2012) [arXiv:1210.5070 [hep-ex]].

[14] G. Aad *et al.* [ATLAS Collaboration], JHEP **1206**, 039 (2012) [arXiv:1204.2760 [hep-ex]].

[15] G. Aad *et al.* [ATLAS Collaboration], JHEP **1303**, 076 (2013) [arXiv:1212.3572 [hep-ex]].

[16] G. Aad *et al.* [ATLAS Collaboration], Eur. Phys. J. C **73**, no. 6, 2465 (2013) [arXiv:1302.3694 [hep-ex]].

[17] S. Chatrchyan *et al.* [CMS Collaboration], JHEP **1207**, 143 (2012) [arXiv:1205.5736 [hep-ex]].

[18] G. Aad *et al.* [ATLAS Collaboration], JHEP **1503**, 088 (2015) [arXiv:1412.6663 [hep-ex]].

[19] V. Khachatryan *et al.* [CMS Collaboration], JHEP **1512**, 178 (2015) [arXiv:1510.04252 [hep-ex]].

ex]].

- [20] V. Khachatryan *et al.* [CMS Collaboration], JHEP **1511**, 018 (2015) [arXiv:1508.07774 [hep-ex]].
- [21] A. G. Akeroyd, S. Moretti, K. Yagyu and E. Yildirim, arXiv:1605.05881 [hep-ph].
- [22] A. G. Akeroyd *et al.*, arXiv:1607.01320 [hep-ph].
- [23] A. Arhrib, R. Benbrik and S. Moretti, arXiv:1607.02402 [hep-ph].
- [24] C. Degrande, R. Frederix, V. Hirschi, M. Ubiali, M. Wiesemann and M. Zaro, arXiv:1607.05291 [hep-ph].
- [25] V. Khachatryan *et al.* [CMS Collaboration], Phys. Lett. B **759**, 369 (2016) [arXiv:1603.02991 [hep-ex]].
- [26] A. Belyaev, N. D. Christensen and A. Pukhov, Comput. Phys. Commun. **184**, 1729 (2013) [arXiv:1207.6082 [hep-ph]].
- [27] P. M. Nadolsky, H. L. Lai, Q. H. Cao, J. Huston, J. Pumplin, D. Stump, W. K. Tung and C.-P. Yuan, Phys. Rev. D **78**, 013004 (2008) [arXiv:0802.0007 [hep-ph]].
- [28] K. A. Olive *et al.* [Particle Data Group Collaboration], Chin. Phys. C **38**, 090001 (2014).
- [29] J. Alwall *et al.*, JHEP **1407**, 079 (2014) [arXiv:1405.0301 [hep-ph]].
- [30] A. Alloul, N. D. Christensen, C. Degrande, C. Duhr and B. Fuks, Comput. Phys. Commun. **185**, 2250 (2014) [arXiv:1310.1921 [hep-ph]].
- [31] T. Sjostrand, S. Mrenna, P. Z. Skands, JHEP **0605**, 026 (2006).
- [32] C. S. Deans [NNPDF Collaboration], arXiv:1304.2781 [hep-ph].
- [33] <http://www.physics.ucdavis.edu/conway/research/software/pgs/pgs4-general.htm>.
- [34] J. Alwall and J. Rathsman, JHEP **0412**, 050 (2004) [hep-ph/0409094].
- [35] S. Hoeche, F. Krauss, N. Lavesson, L. Lonnblad, M. Mangano, A. Schalicke and S. Schumann, hep-ph/0602031.
- [36] M. L. Mangano, M. Moretti, F. Piccinini and M. Treccani, JHEP **0701**, 013 (2007) [hep-ph/0611129].
- [37] M. Aaboud *et al.* [ATLAS Collaboration], Phys. Lett. B **759**, 555 (2016) [arXiv:1603.09203 [hep-ex]].